Microfibrillated cellulose as a new approach to develop lightweight cementitious composites

Taheri, H.; Mastali, M.; Falah, M.; Abdollahnejad, Z.; Ghiassi, B.; Perrot, A.; Kawashima, S.

DOI:
10.1016/j.conbuildmat.2022.128008

Document Version
Peer reviewed version

Citation for published version (Harvard):
Taheri, H, Mastali, M, Falah, M, Abdollahnejad, Z, Ghiassi, B, Perrot, A & Kawashima, S 2022, 'Microfibrillated cellulose as a new approach to develop lightweight cementitious composites: rheological, mechanical, and microstructure perspectives', *Construction and Building Materials*, vol. 342, Part A, 128008. https://doi.org/10.1016/j.conbuildmat.2022.128008

Construction and Building Materials

Microfibrillated cellulose as a new approach to develop lightweight cementitious composites: Rheological, Mechanical, and Microstructure Perspectives

Hesam Taheri [a, g*], *Mohammad Mastali* [b], *Mahroo Falah* [c, d], *Zahra Abdollahnejad* [e], *Bahman Ghiassi* [f], *Arnaud Perrot* [a], *Shiho Kawashima* [g]

[a] Université de Bretagne Sud, FRE CNRS 3744, IRDL, Lorient, France

[b] Durham School of Architectural Engineering and Construction, University of Nebraska-Lincoln, Omaha, NE 68182, USA

[c] Fibre and Particle Engineering, Faculty of Technology, University of Oulu, 90014 Oulu, Finland

[d] Betolar oy, Center of Green Building Technologies Ltd., Mannilantie 9, 43300 Kannonkoski, Finland

[e] Civil & Environmental Engineering Department, University of Connecticut, 261 Glenbrook Road Unit 3037, Storrs, CT 06269-3037, USA

[f] School of Engineering, Department of Civil engineering, University of Birmingham, Edgbaston B15 2TT, Birmingham, United Kingdom

[g] Columbia University, Department of Civil Engineering and Engineering Mechanics, 500 West 120th street, New York, NY, 10027, USA

*Corresponding author: hesam.taheri@univ-ubs.fr

Abstract

Lightweight cementitious composites have a broad range of applications, such as filling or thermal insulation, and should display minimal mechanical properties. Our approach was to prepare mixtures of ordinary Portland cement (OPC) and micro- and nanofibrillated cellulose (CNF) at different water to cement ratios (W/C) to optimize a composite with low density, and either high compressive or flexural strength. The rheological data of W/C =1 CNF-OPC paste confirmed that the viscosity and yield stress of the sample containing 1.1 wt% cellulose fiber was abruptly increased in comparison to the sample without fibers. The results also confirmed the well miscibility (dispersion/distribution) of the OPC in high-water content (98 wt%) fiber medium due to absence of aggregation or agglomeration signatures in plotted rheological data. The dry densities of the CNF-OPC specimen were obviously reduced from 800 kg/m^3 to 450 kg/m^3 by increasing the content of fiber from 1.1 wt% (W/C=1) to 1.8 wt% (W/C = 4), respectively. However, the compressive strengths of the CNF-OPC mixtures were dramatically dropped at higher W/C. Based on the results of mechanical testing, the used lightening technique had less effect on flexural strength loss compared to that of compressive strength, which is related to the bridging action of micro- and nanofibrillated cellulose in the matrix.

Keywords: Micro- and nanofibrillated cellulose, cement, lightweight-composite, rheology.

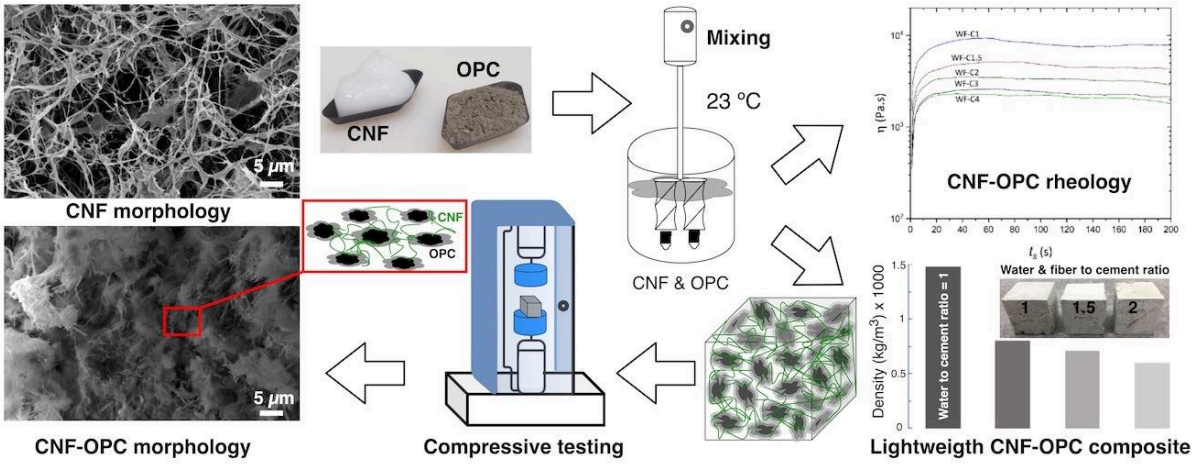

Synopsis. Preparation of microfibrillated cellulose-ordinary Portland cement composites (CNF-OPC). CNF-OPC morphology, rheology and strength characterization.

1. Introduction

Today we are living in global warming crisis due to the emission of carbon dioxide, fossil fuel burning, and cement production. There is an essential need to decrease the volume of these sources to move toward zero carbon emission (1). Therefore, the use of bio-based materials such as cellulose can be directly or indirectly played an important role to decrease the global warming. The abundance of cellulosic materials such as wood, wood pulps and waste or by-products of industry (2) with annual production exceeding 1 trillion tons (3), along with their extraordinary physical, chemical (4), optical (5), and mechanical properties (6) in the nanoscale range, make cellulose and, in particular, cellulose nanofibers interesting for scientists and put them into the spotlight. Different descriptions of these nanoscale fibers are referred to in the literature: (i) cellulose nanowhiskers (CNW) or cellulose nanocrystals (CNC) are designated to represent short crystalline rod-like nanoparticles, while (ii) micro- and nanofibrillated cellulose (MFC) or (CNF) are termed to designate long flexible nanoparticles with either micro- or nanoscale fiber diameters, consisting of alternating crystalline and amorphous domains (7).

Novel processing methods are used to extract cellulose nanofibers by defibrillation of cellulose resources into different micro- and nanoscale morphologies. The so-called none-toxic micro- and nanofibrillated cellulose (CNF) gel-like products are mostly processed by grinding (8) (9) (10), homogenization/microfluidization (11) (12), and TEMPO-oxidation (13). The main issues of these methods are cost, very low fiber contents of around 2-5 wt% for CNF, hornification of the fibers as a result of drying of the gel, redispersion issues (e.g., for CNC) (14) and flocculation or aggregation of fibers within hydrophobic matrices, which affects the mechanical properties of the composites. However, the cost of CNF has been decreased due to market request and large-scale production. Moreover, the CNF gel with high water content has hydrophilic behavior which is causes by some dispersive and distributive barriers when they are compounded with a hydrophobic (bio)polymer (15). Twin-screw extrusion (TSE) as an alternative method has been recently used by scientists in the last decade to defibrillate cellulose fibers and to overcome the aforementioned solid content and cost issues (16) (17) (18) (19). However, poor dispersive and distributive mixing remains as a disadvantage of hydrophilic cellulose fibers (20).

The simple scenario of the cementitious or clay material is on the opposite side of the (bio)polymers extrusion process, as cement slurry consists of 25-50 wt% water. In other words,

the disadvantage of CNF gel (high water content) can be grasped as an advantage and can be used for preparing fiber-cement mixtures. Therefore, there is high potential to use bio-based materials, such as CNF gel, which give rise to high-volume surface fiber networks that might improve the flow behavior of the fiber-cement mixtures (fresh properties, rheology, resistance to bleeding), density, crack resistance due to drying, and mechanical properties after processing and curing.

There are several but not many works that show the beneficial effects of CNF when added as reinforcement or as additive to cementitious matrices. Mejdoub et al. (21) reported enhanced mechanical and thermal properties of CNF-cement systems compared to the control. Ardanuy et al. (22) observed that the flexural strength of CNF-cementitious composites increases nearly two-fold in comparison with cellulose-cement composites. Enhanced mechanical properties have also been reported by Onuaguluchi et al. (23) when the CNF fibers were added to cement at 0.05-0.4% additions. In another study the setting time and the degree of hydration of CNF-cement composite increases with increasing proportions of CNF up to 0.2% (24). Improvements have also been reported for the energy absorption property and wet/dry cycling durability of CNF-cement composites (22) (23). The addition of CNF has been found to cause increase in yield stress of fresh CNF-cement slurries, and the Vom Berg model provided the best fit for the shear rate-shear stress flow curve (25) (26). Tang et al. (24) reported that the gel strength, yield stress and viscosity of the CNF-cement increased due to the formation of an entangled fiber network. The same authors reported that the quality of the used CNF alters the strength of the cement paste and changes in rheological properties.

Even though the amount of fiber content in CNF materials is very low (around 2-5 wt%), the CNF gel shows a bulky behavior due to the high specific surface area of the fibers. Therefore, it can be expected that the density of CNF-cement composites decreases and shows the behavior of lightweight cement composites or foam concretes, wherein the air voids are entrapped into the cementitious matrix and confined within the binding skeleton to drop the density of the matrix during the setting and hardening stages (27). The advantages of light weight cement composites can be reflected in the thermal and acoustic insulation properties, structural weight reduction, and easy transportation and assemblage (28) (29). Different methods such as mechanical foaming (30) (31) and chemical foaming techniques (32) (33) have been used to generate the air voids into the cementitious matrix. However, other approaches such as alkali-activated materials have also been

used to produce light weight cement-based composites due to their ecofriendly features (34). Therefore, bio-based CNF materials can be highlighted as an important alternative due to their beneficial effects on the sustainability, density, porosity, fresh property, rheological behavior, and mechanical properties of light weight fiber-cement composites.

In this work, microfibrillated cellulose (CNF) was produced and mixed with ordinary Portland cement (OPC) in different fiber proportions and water to cement ratios (W/C). The novel idea in this work is related to using the existing water in CNF gel, thus any extra water was not added to the composite mixtures. The primary goal of this work was aimed to tune the rheological changes of the mixtures due to different parameters such as shear rate and time evolution. The secondary goal was to prepare CNF-OPC composites with different fiber contents and W/C, to ultimately produce light weight cement composites with optimum mechanical properties. The microstructure of obtained CNF-OPC composites were studied to observe how the fibers and cement particles will be mixeed and will affect the properties of CNF-cement composite.

2. Experimental plan

2.1. Materials and methods

Ordinary Portland cement 42.5R with specific chemical composition and physical properties (shown in **Table 1)** was used in this work. Never-dried softwood pulp as the raw source with a solid content of 36-37 wt% (Stora Enso, Oulu, Finland) and chemical composition of 2.45 wt% hemicellulose, 1.5 wt% lignin and 0.5 wt% inorganics (TAPPI-T 222 standard) was used to produce CNF.

Table 1 Chemical composition and physical properties of ordinary Portland cement 42.5R.

Ordinary Portland Cement (OPC-42.5R)												
Physical properties		**Chemical composition (%)**										
Specific gravity	Specific surface (cm^2/g)	SiO_2	Al_2O_3	Fe_2O_3	MgO	K_2O	Na_2O	CaO	C_3S	C_2S	C_3A	C_4AF
3.11	300	21.1	4.37	3.88	1.56	0.52	0.39	63.33	51	22.7	5.1	11.9

The softwood pulp was soaked in water and processed by a Masuko super masscolloider MKCA6-2J (Japan) grinder. The Masuko grinder's stones were firstly closed in a tiny gap as long as the low friction zero gap to be confirmed. Then the soaked pulp slurry was poured into the grinder at a consistency of 2.3 wt%. The fiber slurry was passed three times through the grinder using a zero-

grinding stone gap; then, the stones were adjusted to negative gap values to fibrillate the pulp fibers. The process was repeated three times with -20 μm stone gap, three times with -40 μm stone gap, three times with -60 μm stone gap, and additional nine passes with -90 μm stone gap. The prepared CNF was mixed with OPC based on the samples' formulation (shown in **Table 2**) by a two-propeller mixer at a speed of 300 rpm for 10 minutes. The prepared samples were loaded in a mold or vane rheometer cup and vibrated for 1 minute. Two different molds (50 × 50 × 50) mm^3 and (40 × 40 × 160) mm^3 were used to measure density and mechanical properties after 28 days, respectively.

Table 2 Sample formulation and coding of material compositions and preparation methods.

Sample	CNF		OPC (wt%)	Total (wt%)	Water to cement ratio (W/C)
	Water (wt%)	Fiber (wt%)			
CNF*	97.7	2.3	0	100	N/A
W-C1	50	0	50	100	1
W-C1.5	60	0	40	100	1.5
W-C2**	66.7	0	33.3	100	2
WF-C1	49.4	1.1	49.4	100	1
WF-C1.5	59.3	1.3	39.4	100	1.5
WF-C2	66.5	1.5	32	100	2
WF-C3	73.8	1.7	24.5	100	3
WF-C4	78.7	1.8	19.5	100	4

* The sample was used for FE-SEM.
** The maximum W/C can be reached without fiber even with sedimentation.

2.2. Test procedures

2.2.1. Rheometry

The rheological measurements of cement paste and CNF-OPC mixtures were done using a TA Instrument Discovery HR-1 Hybrid Rheometer (New Castle, DE, USA). Different mixtures were prepared based on the prior formulations presented in **Table 2** to compare the flow behavior of the bulk cement paste without fibers against those of the CNF-OPC pastes. The rheological behavior of the samples under the strain-controlled mode was measured by vane rotor and grooved cup accessories. The steady state shear-viscosity, time sweep, and frequency sweep tests were done to investigate the rheological properties of bulk CNF-OPC mixtures at 23 °C. The wall-slip effect of the test protocol for the used medium was also checked at three different gaps (5000 ± 1000 μm), and the shear-viscosity data were regenerated at all gaps, confirming the absence of wall-slip. The reference gap of 5000 μm was fixed for all experiments, and the gap was slowly adjusted within 2

minutes to erase additional stress and equilibrate the temperature between the sample and grooved cup. The steady state shear-viscosity tests were done under a controlled shear rate in an ascending and descending sequence of about 10 minutes (5 minutes for ramp-up then 5 minutes for ramp-down) to show the flow behavior within the shear rate interval of 0.1 to 1000 s^{-1} at 23 °C. The time sweep tests were done under very low constant shear rate (0.1 s^{-1}) over 150 minutes to study the hardening evolution of the mixtures. The linear regime of two samples was shortly checked via strain sweep tests. Based on these results, a constant strain of 0.5% was used in the frequency sweep tests, which were performed in the range of 0.1 to 100 $rad.s^{-1}$. The frequency sweep test data was overlapped with steady state shear viscosity data to observe if the cement paste and CNF-OPC composites will follow the Cox-Merz rule (35). The total preparation time for each sample was recorded from the first contact of cement and water and included the subsequent steps of mixing, vibrating, loading, and adjusting in grooved cup, and was controlled to be around 15 ± 0.2 minutes.

2.2.2. Flexural and compressive strength

The molded cement paste and CNF-OPC samples were tested under three-point bending (TPB) load conditions by using the ASTM C78 recommendation (36). The flexural load was applied to the beams at a displacement rate of 0.6 mm/min and a loading cell under 100 kN force. The flexural load was recorded by using a Zwick, Z100 Roell testing machine (Ulm, Germany) and calculated using the following equation:

$$\sigma_f = \frac{3FL}{2bh^2} \quad (1)$$

where F is the total flexural load, L is span length (160 mm), b and h are width (40 mm) and height (40 mm) of beams, respectively. The compressive strength was measured by using the ASTM C349 recommendation for cube samples after having air dried for 28 days (37). The compressive load was applied with a displacement rate of 1.8 mm/min. For each CNF-OPC sample, the flexural and compressive strengths represent the average of the five measurements. Moreover, the dry densities of CNF-OPC compositions were obtained by drying the cube samples (50 × 50 × 50) mm^3 at 105 ± 2 °C in an oven for 24 hours by using the ASTM C567 recommendation (38).

2.2.3. Microstructural analysis

FE-SEM-EDS: Energy-dispersive X-ray spectroscopy (EDX) was used to study the chemical characterization/elemental analysis of the samples. The sample is excited by an energy source and dissipates some of the absorbed energy by ejecting a core-shell electron. A higher energy outer-shell electron then proceeds to fill its place, releasing the difference in energy as an X-ray that has a characteristic spectrum based on its atom of origin. The position of the peaks in the spectrum identifies the element, whereas the intensity of the signal corresponds to the concentration of the element. Compositional information, down to the atomic level, can be obtained with the addition of an EDS detector to an electron microscope. As the electron probe is scanned across the sample, characteristic X-rays are emitted and measured; each recorded EDS spectrum is mapped to a specific position on the sample.

FE-SEM: Field emission scanning electron microscopy (ZEISS ULTRA plus FE-SEM, Carl Zeiss AG, Oberkochen, Germany) was used to study the microstructure of neat CNF and CNF-OPC samples. The collected CNF-OPC mixtures were firstly dried at 100 ± 5 °C in an oven for 6 hours. The samples were mounted on sample holders and platinum-coated before FE-SEM to avoid charging. An acceleration voltage of 5 kV was used with the measurement distance of 6–8 mm.

3. Results and discussion

3.1. Flow properties

3.1.1. Steady state mode rheology

The steady state ascending/descending shear-viscosity tests of the cement paste and CNF-OPC were examined with equal W/C to understand the effect of CNF on the rheological behavior of the mixtures. As shown in **Fig. 1a**, the ascending shear-viscosity plot of cement paste (W-C1) at low shear rate interval (0.1 s^{-1}) was abruptly increased from 8 Pa.s to 4000 Pa.s when 1.1 wt% cellulose nanofiber (WF-C1) was added to the mixture at a fixed W/C = 1. The flow properties of both samples (W-C1 and WF-C1) are showing a shear thinning behavior and the viscosity trend of the sample that contains CNF was greater – around 100x at intermediate and high shear rate intervals. The increase of the viscosity can be related to the fiber-fiber entanglement and likely networks between cement and nanofibers. The descending shear rate depicted a hysteresis for both samples with equal W/C. However, the hysteresis at low shear rate for the sample with CNF was greater than the sample without CNF, which is related to a competition between the fibers' network history

and hardening of the cement matrix within 25 minutes. Moreover, any packing phenomenon or abrupt shear thickening behavior was not observed at low and intermediate interval confirming well dispersive mixing and absence of aggregation. With increase in fiber amount (WF-C2), the hysteresis of the ramp up and ramp down data at intermediate shear rates (10-15 s^{-1}) was decreased where the smooth plateau going to be formed. In contrast, the ramp up and ramp down data for the cement mixture (W-C2) showed greater hysteresis at intermediate shear rates due to the absence of fiber cement interactions. The observed difference can also be explained by the instability (bleeding) of the mixture without CNF. The rheological change was clearly pronounced the fiber-cement network while even at higher W/C = 2, the sample with 1.5 wt% cellulose nanofiber (WF-C2) showed a greater ascending/descending viscosity trend in comparison with cement paste at W/C = 1 (W-C1) (**Fig. 1a**). As the amount of cement in WF-C1 is greater than the amount of cement in WF-C2, the viscosity of WF-C1 at low shear rate interval (0.1 s^{-1}) remained two times higher than that of WF-C2. According to **Fig. 1a**, with increasing cellulose nanofiber content from 1.1 wt% (WF-C1) to 1.5 wt% (WF-C2), the rheological properties of CNF gel start to be more dominant than that of cement, as indicated by the so-called plateau of the curve at intermediate shear rate (15 s^{-1}); serving as a fingerprint of CNF rheological behavior (12).

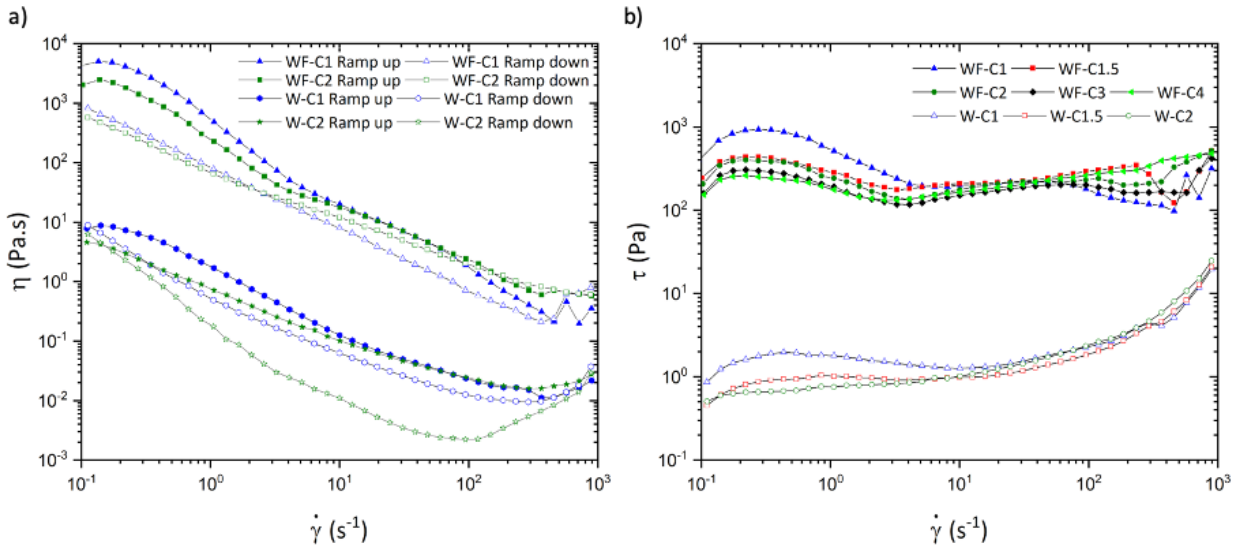

Fig. 1. The comparison of flow behavior of cement paste and CNF-OPC mixtures at 23 °C. a) shear versus viscosity plots, solid and open symbols indicate ascending (ramp up) and descending (ramp down) shear rate, respectively; b) shear rate versus stress.

As shown in **Fig. 1b**, the alteration of yield stress for the cement paste and CNF-OPC with different W/C was studied. The yield stress (τ_0) was defined as the peak of the shear versus stress curve (39) at low shear rate interval (0.1–1 s^{-1}), while the plastic viscosity (η_{pl}) can be computed as the slope of a linear fit (40) at intermediate shear rate interval (10–100 s^{-1}). The yield stress of CNF-OPC composites with different W/C (or fiber proportion) were identified as around 927, 437, 400, 305, and 261 (Pa) for WF-C1, WFC1.5, WF-C2, WF-C3, and WF-C4 samples, respectively. The mentioned peak can be defined for cement paste samples with W/C = 1 and 1.5 as around 1.9 and 1.1 (Pa), respectively. The comparison of plastic viscosity of W-C1 (η_{pl} = 0.02 Pa.s) and WF-C1 (η_{pl} = 6.79 Pa.s) is confirming the significant effect of the nanofibers on flow behavior. Based on **Fig. 1b**, the increase in CNF from 1.1 to 1.5 wt% decreases the yield stress of the mixture as the W/C was increased. However, the absence of CNF with equal W/C resulted in very low yield stress. Therefore, it can be predicted to tune the greater yield stress using CNF in a lower W/C, which is remarkable for processing applications such as 3D printing (39).

The time-dependent response of the CNF-OPC composites at constant shear rate (0.1 s^{-1}) are shown in **Fig. 2** to understand the stress evolution of the samples. At early ages (around 90 seconds), the stress and viscosity trends of all CNF-OPC samples were increased due to the increase of the strain imposed by the test conditions until a peak value or a plateau is reached (**Fig. 2a**). In this phase, the material behaves as an elastic solid. The time at which the plateau or the peak is reached is almost the same, meaning that the critical strain does not depend on W/C. At later age, the shear stress of WF-C1 was decreased to reach an equilibrium value (at around 2500-8000 seconds) which is the signature of an unstructured flowing material. This response is obviously different from the neat cement paste with W/C = 1, whereas the stress increases was observed due to hardening and also reported in other works (41). This difference can be attributed to the retarding effect brought by the CNF. However, the shear thinning behavior of the other samples with greater W/C continued to decrease and the mentioned equilibrium occurred within the time frame of 6000-7000 seconds, where the hydration effect and structural build-up of cement is only happening at these times.

The fluctuation of stress data and the saw-tooth response can be related to breakdown/recovery of the fiber-fiber entanglements, fiber-cement networks, and interparticle forces of the mixtures (**Fig. 2b**). However, the same behaviors such as the initial shear thinning and saw-tooth response have

been reported as microstructural breakdown in the material under applied shear rate (41). In brief, the CNF-OPC composite with W/C = 1 showed the highest yield stress among the samples and the normalized time-dependent stress remained constant (350-400 Pa) during the time window of 2500-8000 seconds. However, the stress values increased after 8000 seconds confirming the chemical reaction of the composite and hardening of the mixture. At higher W/C = 2, 3, and 4, it was obvious that the mentioned linear stress equilibrium occurred at later time and the hardening fingerprint was not observed in the experimental time window. Interestingly, at W/C = 1.5 the composites did not reach the linear equilibrium, which can be related to intermolecular competition between the CNF gel and cement particles to dominate their rheological properties. It could be interesting to add setting accelerator to obtain a faster hardening of the CNF added materials close to the one can be observed by neat cement at low W/C.

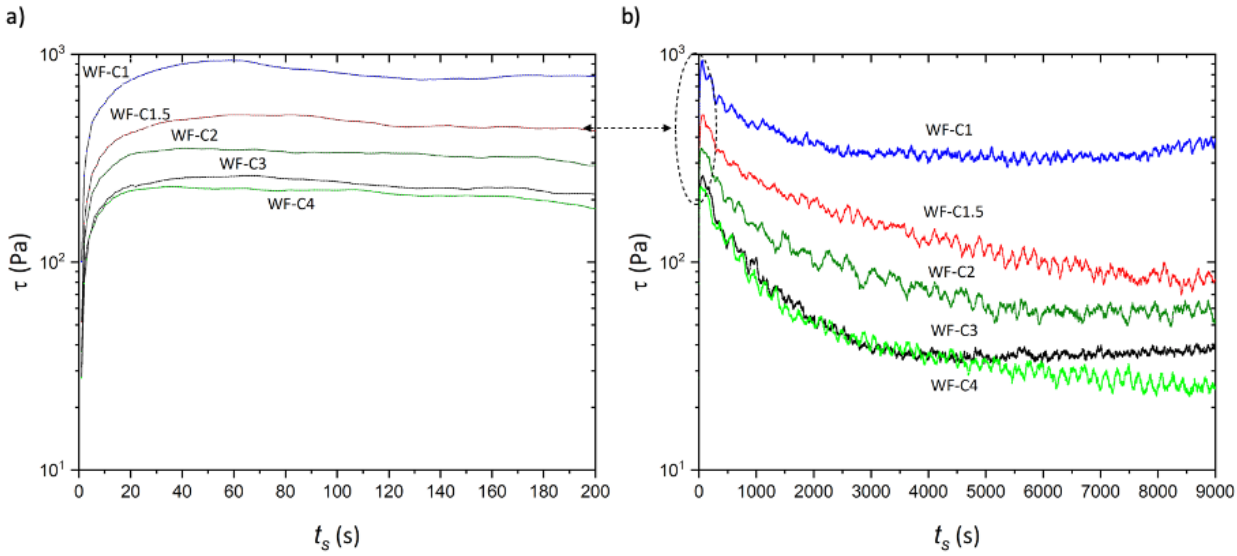

Fig. 2. The evolution of stress as function of time in constant applied shear rate of 0.1 s^{-1} at 23 °C. a) the resolution of the first 200 seconds, b) overall testing time of 9000 seconds.

3.1.2. Dynamic mode rheology

The dynamic properties of CNF-OPC

The dynamic rheology of CNF-OPC composites was measured as a function of frequency at a constant strain of 0.5%, which is significant for processing applications such as extrusion. As shown in **Fig. 3a**, the dynamic behavior of all CNF-OPC composites with different W/C showed a solid-like behavior as the storage modulus (G') was higher than the loss modulus (G").

Furthermore, any cross-over between (G') and (G") for the CNF-OPC composites was not observed and the solid-like component of the mixtures (G') were smoothly increased with increment of frequency. At low frequency the composite with W/C = 1 had a higher (G') value in comparison with other samples. However, the (G') for the sample with W/C = 1.5 and 2 were close within the whole frequency interval. Such result is in agreement with the high yield stress of the samples with CNF.

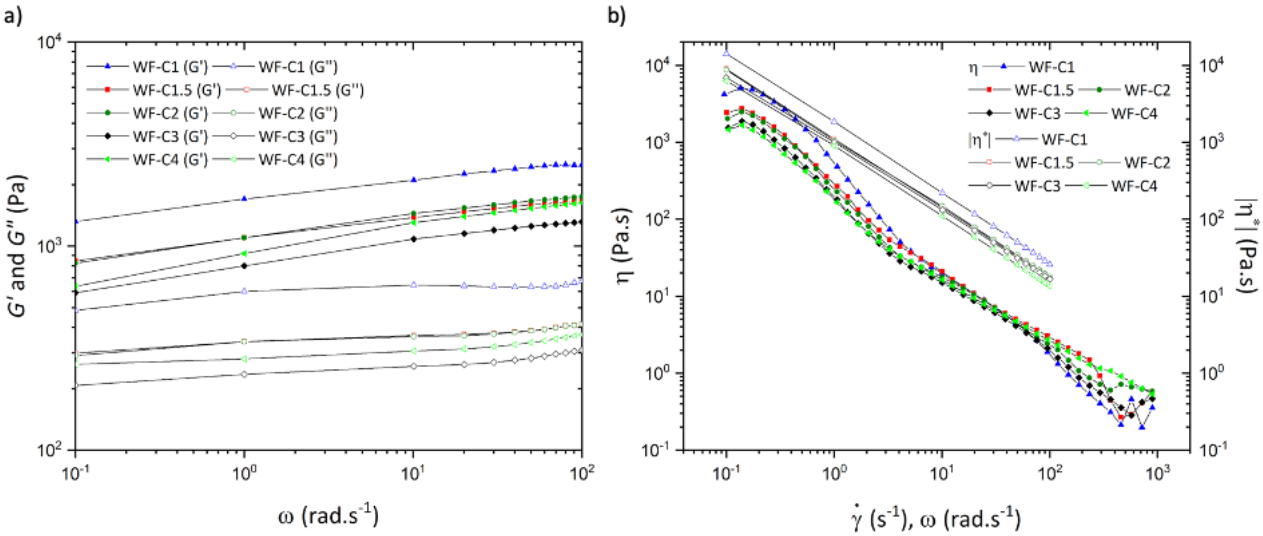

Fig. 3. The steady-state and dynamic rheology of CNF-OPC composites with different W/C at 23 °C. a) frequency sweep test, b) comparison of steady state rheology (solid symbols) and dynamic rheology (open symbols) due to Cox-Merz rule.

Due to the Cox-Merz rule, the complex viscosity data $|\eta^*(\omega)|$ from dynamic testing can be overlapped with the shear viscosity data $\eta(\dot{\gamma})$ from steady state testing at low shear rates and frequencies (35). In general, this principle is used for molten polymers or highly dense particle mediums, which is remarkable for extrusion processing. However, it is interesting to study the cement-based materials response with the so-called Cox-Merz principle, which can be related to extrusion or 3D printing applications. As shown in **Fig. 3b**, the plotted data of CNF-OPC composites at $|\eta^*(\omega)| = \eta(\dot{\gamma})$ does not show any overlapping of steady state and dynamic data. However, the shear viscosity and complex viscosity of the CNF-OPC composite with low W/C = 1 are close at low shear rate or frequency. It can be assumed that with decrement of W/C the fiber-cement mixture shows more dense properties and the mentioned rule can be applied for cement-based materials. However, the main reasons for the steady state and dynamic data deviations might

be related to the presence of intra- and inter-molecular hydrogen bonds or the negative charges of the cellulose nanofiber particles in the cement matrix.

3.2. Dry density

One of the main important indices to assess lightweight cementitious compositions is dry density. Lighter material reflects higher porosity, although this does not reflect the pore structure (size and distribution of pores) of the matrix. As the dry density of the used OPC without CNF (W/C = 1) is 1480 kg/m^3, **Fig. 4a** shows the influence of adding CNF to the cementitious pastes. Dry densities of the mixtures were consistently reduced from 800 kg/m^3 to 450 kg/m^3 by increasing the content of CNF from 1.1 to 1.8, respectively. In order to obtain a lightweight construction material, the dry density should be lower than 1000 kg/m^3, and all developed materials in this study meet this important requirement. Additionally, as shown in **Fig. 4b**, a nonlinear correlation was developed between density and W/C with a high coefficient of determination ($R^2 \geq 0.96$).

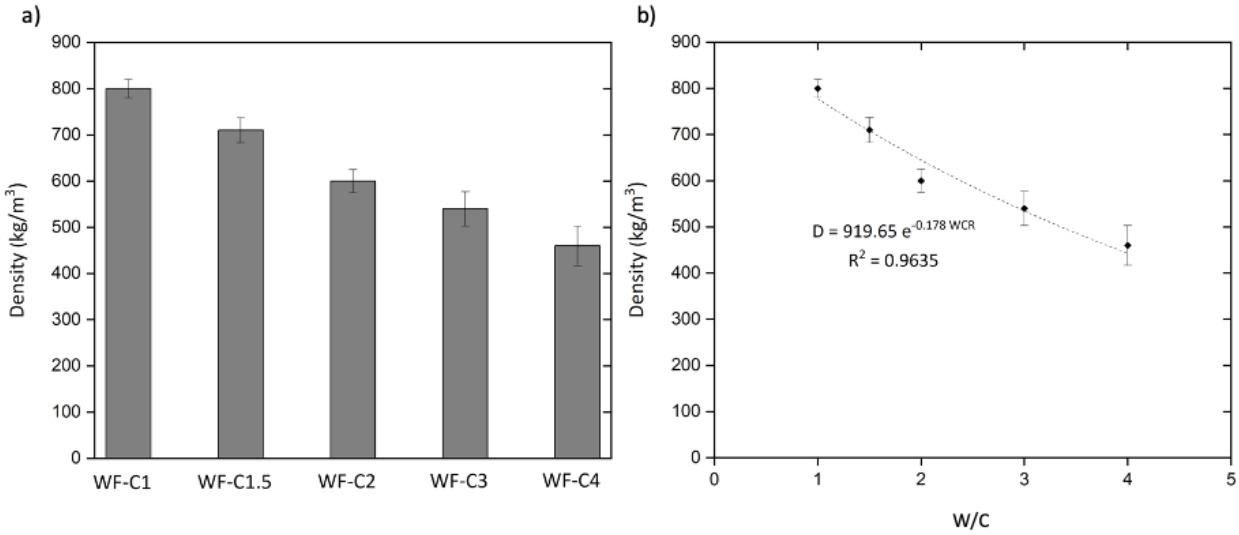

Fig. 4. a) Dry density of the mixtures containing different contents of CNF, b) correlation between density and water to cement ratio.

3.3. Compressive and flexural strength

Lightening the cementitious materials degrades the mechanical strength of the lightweight composites due to the porous structure of the material, where this strength loss mainly depends on the lightering technique. Evaporation of free water from cementitious compositions, once set, results in an increase in porosity of the matrix, as free water does not participate in chemical reactions and so its evaporation leaves voids. Evaporation of high amount of free water results in

forming a porous structure in the matrix. The water evaporation process in mixtures containing CNF has some aspects, including: i) the presence of pulp fibers in CNF provides multiple air channels in the cementitious matrix, which facilitates the removal process of free water from the matrix, and the formation of pores in the matrix; ii) the presence of CNF provides a physical confinement system in the cementitious matrix and, this confinement leads to slowed evaporation of water from the cementitious matrix; iii) good interaction of pulp fibers with water during the preparation process of CNF submits new constrains for slowed evaporation of free water. The first mechanism results in air entering the matrix and generating fine pores within the matrix, while the second and third mechanisms reduces the rate of free water evaporation from the matrix at the early ages of casting. The first mechanism can be effective in obtaining a lightweight material with a high number of fine pores. Additionally, the slowed water evaporation leads to convert a weak amount of remaining free water into gel water at the early age of casting, which prolonged significantly the setting time of these lightweight materials. This prolongation makes them completely appropriate for casting in real applications.

Fig. 5 indicates the influence of adding different contents of CNF on the mechanical strength of the cementitious compositions. Increasing CNF to cement ratio (and therefore W/C) forms more fine pores, and degrades the mechanical strength compared to the mixtures containing lower amounts of CNF (and lower W/C). As expected, both compressive and flexural strength consistently decreased with increasing amount of CNF and W/C so that the compressive strength varied from 7.5-1 MPa for mixtures containing CNF 1.1-1.8 %, respectively, as shown in **Fig. 5a**. Furthermore, the flexural strength changed from 3.6-1 MPa for mixtures containing CNF 1-4, respectively. Comparing the developed strength for the lightweight materials with their reference cementitious pastes in **Fig. 5b** revealed that the used lightering technique has less effect on flexural strength loss compared to that of compressive strength. This is due to the bridging action of micro- and nanofibrillated cellulose in the matrix. It was also visually observed that the presence of CNF (regardless of its content) had a significant impact on mitigating drying shrinkage to prevent cracking. The plain cementitious compositions with W/C higher than two exhibited significant shrinkage, which resulted in cracks formed on their surfaces. Therefore, measuring the mechanical strength for the plain cementitious compositions with W/C higher than 2 was not possible.

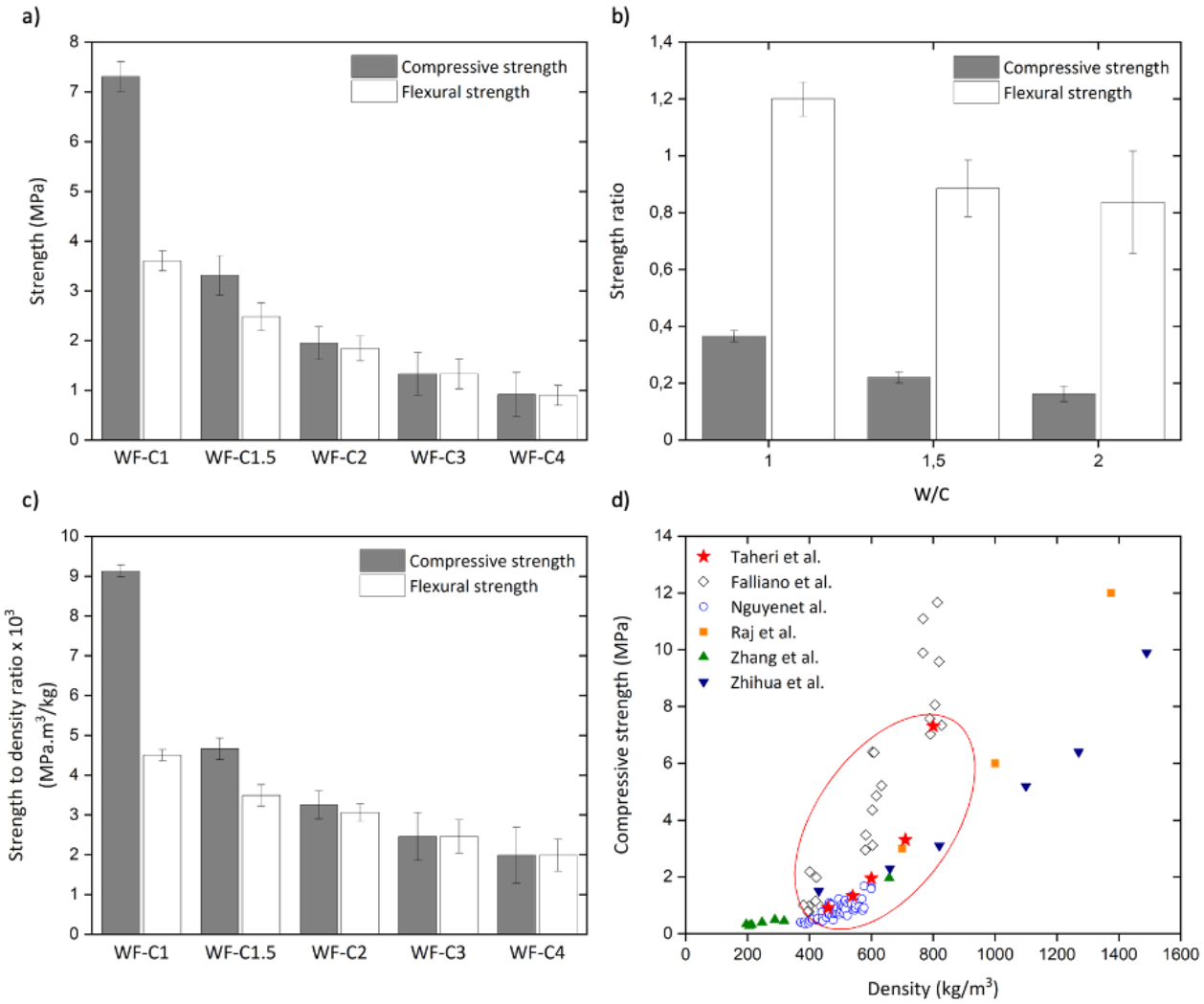

Fig. 5. a) Mechanical strength for mixtures containing different contents of CNF, b) mechanical strength of mixtures containing different contents of CNF to mechanical strength of the reference mixtures without CNF, c) compressive strength to density ratio of mixtures containing different contents of CNF, d) comparison of the compressive strength versus density for different foamed concrete and this work (42) (43) (44) (45) (46).

For lightweight construction materials with density lower than 1000 kg/m^3, the compressive strength to density ratio varies between 0.5-14×10^{-3} MPa.m^3/kg (42) (43). Higher values of this ratio means that the material has higher strength with lower density, which is appropriate for lightweight materials. According to the obtained results in **Fig. 5c**, the compressive strength to density ratio for developed materials through using this lightening technique varied between 2-9×10^{-3} MPa.m^3/kg, which is an acceptable interval. The compressive strength versus density for different lightweight cementitious materials is shown in **Fig. 5d**. Based on the recorded data, the

compressive strength of OPC-based foam concretes is in the range of 0.25–13 MPa for densities in the range of 200–1400 kg/m^3 (44) (45). The compressive strength could have either linear or nonlinear correlation with density.

Accordingly, the compressive strength of the materials developed in this study have a nonlinear correlation with density, and the compressive strength increases with a steep slope beyond a density of 800 kg/m^3. The nonlinear correlation between compressive strength and density in this study is more related to W/C (cement content) and bulk networks of CNF gel. It can be interpreted from the data (star symbols in **Fig. 5d**) that the W/C = 1 is a threshold ratio for the CNF-OPC where the composite has a density lower than 800 kg/m^3 with an optimum compressive strength of 7.4 MPa. Therefore, at the same W/C and without CNF, the density (1480 kg/m^3) and the compressive strength (13 MPa) will be dropped with presence of the fiber networks by 48% and 42% respectively. Increasing of the W/C from 1 to 2 is also caused the decrement of density and compressive strength by 10 % and 55% respectively. In one hand the fiber networks caused the decrement of the density but on the other hand it decreased the compressive strength. In brief, the abrupt decrement of density is occurred at W/C = 1 when the fiber networks are involved and the dramatic strength loss is occurred at W/C = 2 when the fiber networks are increased and cement content decreased. This is a very promising result for this lightening technique, showing the potential to reach high mechanical strengths at densities above 800 kg/m^3 and within 1000 kg/m^3.

3.4. Microstructural and EDS analysis

The FE-SEM images of CNF and CNF-OPC mixtures at different W/C are presented in **Fig. 6**, and they support the findings of the rheological and mechanical investigations. As shown in **Fig. 6a**, the bulk network of microfibrillated cellulose confirmed the high porosity gel with well-distributed voids (1-3 μm) and high aspect ratio fibers (width 100-500 nm and length 5-10 μm). The mentioned networks increased the rheological properties of the CNF-OPC mixtures and decreased the density of the composites. As shown in **Fig. 6b**, some large cement flocs (showed in circle line) were formed with equal W/C and lowest CNF content. While with the increment of CNF proportion in composites, the fiber networks were controlled the forming of large cement flocs or high dense composites (**Fig. 6c-6f**). Based on the mechanical/density results in **Fig. 5d** and micrograph observation **Fig. 6a-6b**, the bulk density of CNF gel is caused the lower density of the composite due to fiber networks. However, the cement ratio was sufficient to form the

coherence connection of the large flocs in CNF-OPC composite and to reach the optimum compressive strength. Unlike, increasing of W/C from 1 to 2 (or decreasing of cement ratio) caused the large flocs turn to smaller flocs and the mixture shifted to form a bulk cement composite. These results are in agreement with 25 % of the density decrement and 62 % of dramatic compressive strength loss due to decreasing of cement ratio (**Fig. 5d** and **Fig. 6d**). Moreover, increasing of W/C ratio (or CNF content) the composite is caused to form highly porous structure as the CNF networks are more dominant in CNF-OPC mixture than cement ratio, which is in agreement of plateau in rheological data. It is remarkable to mention that the large flocs as shown in **Fig. 6b** can be observed as fluctuation or bump at high shear rate interval for steady state rheology shown in **Fig. 1a**. Therefore, the increment of W/C and in follow the fiber content works as barrier to form the large flocs and result in a uniform mixture. Based on the FE- SEM observations, it seems that the CNF networks can be applied as sort of nuclei and the cement matrix forming the composite through the fibers' network. Noteworthy is that the increment of CNF content decreases the density and increases the microcracks in composite, which is the main reason for strength loss (47).

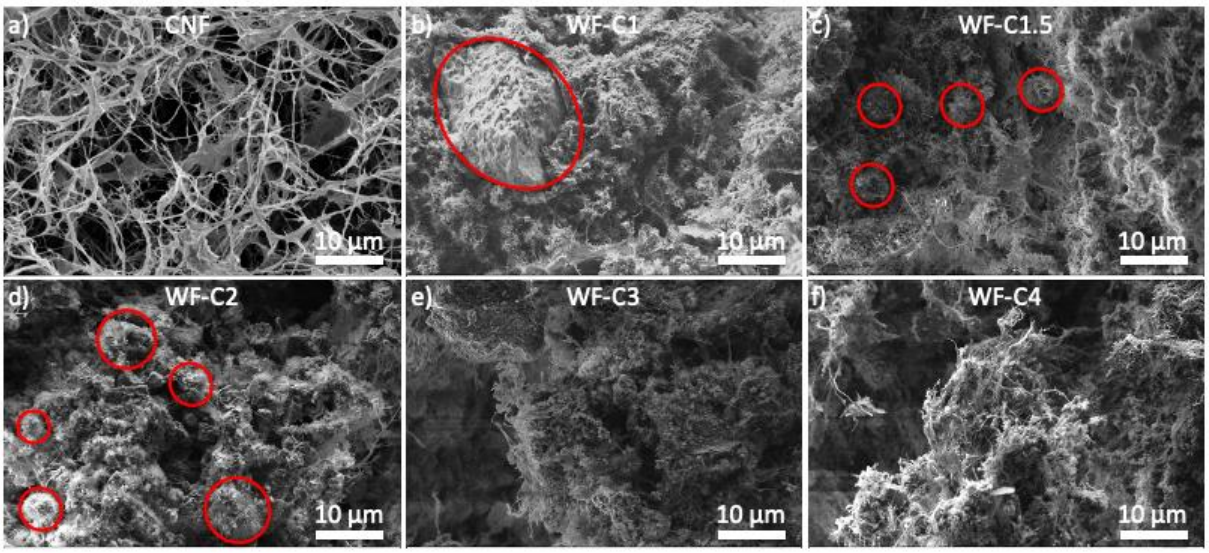

Fig. 6. FE-SEM images of CNF and mixture of CNF-OPC. a) CNF, b) CNF-OPC at W/C=1, c) CNF-OPC at W/C=1.5, d) CNF-OPC at W/C=2, e) CNF-OPC at W/C=3, f) CNF-OPC at W/C=4 (**Table 2**).

A chemical analysis of the air-dried CNF-OPC composite was also performed to observe any possible chemical reactions or critical changes between the main elements of cement and cellulose nanofibers (**Fig. 7** and **Table 3**).

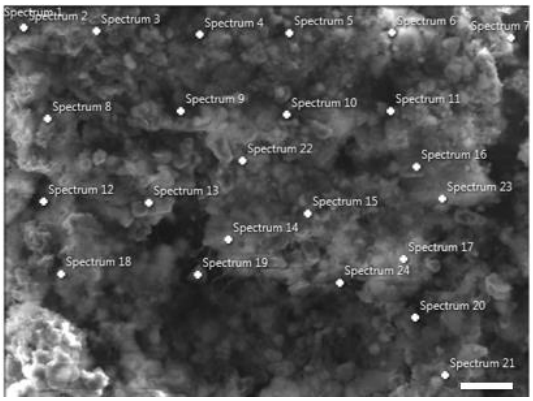

Fig.7. The EDS mapping spectrum of CNF-OPC (W/C = 1). Scale bar is 10 μm.

Table 3 The EDX spectrum for the CNF-OPC (W/C =1).

	Spectrum																								
Label	**1**	**2**	**3**	**4**	**5**	**6**	**7**	**8**	**9**	**10**	**11**	**12**	**13**	**14**	**15**	**16**	**17**	**18**	**19**	**20**	**21**	**22**	**23**	**24**
Na	2,92	2,11	-	3,79	3,5	3,63	1,74	-	-	2,47	3,72	0,9	1,06	3,04	1,84	3,32	3,22	2,25	0,83	-	1,22	2,05	2,88	-
Mg	3,19	1,95	-	5,34	4,21	2,65	2,48	-	-	3,65	3,88	0,83	-	2	2,57	5,44	1,72	1,25	-	-	1,32	1,6	6,27	-
Al	3,91	2,92	-	5,85	5,62	6,54	1,55	3,19	-	4,49	6,93	1,61	-	4,95	2,3	6,58	6,72	5,81	1,13	-	-	4,85	6,11	-
Si	29,5	19,95	1,63	38,08	35,72	43,59	13,36	22,02	5,92	40,06	53,5	16,78	8,44	38,25	14,14	44,73	50,17	48,92	8,41	5,6	8,73	42,37	44,99	3,42
K	2,64	1,24	-	3,05	2,84	3,48	1,05	1,22	-	3,46	3,88	3,43	-	4,01	1,23	3,47	3,69	5,63	1,32	-	0,9	4,74	4,39	3,97
Ca	54,36	71,83	98,37	37,83	46,01	36,62	79,82	70,73	94,08	42,23	23,69	73,52	90,5	44,24	76,13	31,76	30,7	31,86	88,3	94,4	87,83	39,41	30,37	92,61
Fe	3,48	-	-	6,06	2,09	3,49	-	2,84	-	3,64	4,39	2,93	-	3,5	1,79	4,71	3,79	4,27	-	-	-	4,98	4,98	-
Total	100	100	100	100	100	100	100	100	100	100	100	100	100	100	100	100	100	100	100	100	100	100	100	100

In this regard, the EDX spectrums were monitored for the sample with an equal proportion of water and cement (W/C = 1) to observe the probable changes in the samples, as shown in **Fig. 7** and **Table 3**. In one hand, the main chemical bonds of cellulose contain carbon, hydrogen and oxygen and on the other hand, the main chemical bonds of cement paste contain calcium, silica and hydrogen (C-S-H). As there is not any calcium and silica in the CNF gel, CNF can affect C-S-H

gel thorough their hydrogen bonds. EDS analysis showed that the main chemical components of the CNF-OPC mixture is related to calcium (average 61.13%) and silica (average 26.59%), which are the main components can significantly alter the strength. Moreover, EDS analysis can elucidate that the mineral chemical component of the mixture hydrogen bonds in C-S-H can be affected by either water or the hydrogen bonds of CNF. The topography images (FE-SEM) confirmed that the quality of C-S-H gels did not change significantly. As the content of CNF compare to cement-water is low, therefore the amount of hydrogen supplied be CNF will be low. It is noteworthy to mention that the low amount of CNF (less than 0.5 wt%) will increase the degree of hydration and compressive strength of the CNF-OPC composite (47). Therefore, the 1 wt% CNF content (in this work) did not increase the degree of hydration and strength, which has been already confirmed by rheological and mechanical data. Accordingly, it was observed that cellulose fibers had no significant contribution in forming calcium silicate hydrate (C-S-H) as the main product of the hydration of OPC and primarily responsible for the strength gaining. However, degree of hydration, durability and crystallinity of such system (CNF-OPC) needs to be studied in further study.

4. Conclusions

In this study, the preparation of super lightweight cementitious composite with eco-friendly cellulose nanofibers was investigated. Based on rheological and morphological results, the CNF gel and OPC were well dispersed/distributed as no flow fluctuation can be observed at low and intermediate shear rates, and this was confirmed by micrograph observations. The mixture of CNF gel and OPC resulted in an abrupt increase in yield stress and viscosity, which can be attributed to cellulose networks and good distribution/dispersion of cement within the CNF-gel-voids. The mentioned voids played a key role in keeping the cement particles and further decreasing the dry density of the composite, which was reduced from 800 to 450 kg/m^3 with increasing W/C from 1 to 4, respectively. In general, the use of CNF gel degraded the mechanical strength, where the loss of compressive strength was greater than that of flexural strength in comparison with the reference sample at equal W/C due to the bridging action of micro- and nanofibrillated cellulose in the matrix. With a dry density within the interval of 450-800 kg/m^3, a compressive strength of 7.5-1 MPa, and a flexural strength of 3.6-1 MPa, the developed CNF-OPC lightweight composites are adequate for use as construction building materials for lightweight applications. Additionally,

using CNF-gel significantly controlled the drying shrinkage of the composites at all W/Cs as visually observed. Microstructural analysis of the cementitious compositions also revealed that cellulose fibers had no major contribution in forming the hydration products of OPC.

5. Acknowledgments

This project received funding from the Research Executive Agency of European Union's Horizon 2020 research and innovation programme under the Marie Skłodowska-Curie grant agreement No. 101024074. The authors would like to thank Mr. Jarno Karvonen, Mr. Jani Österlund, and Mrs. Elisa Wirkkala for their helps at the Fibre and Particle Engineering Laboratory. Mr. Mohammad Karzarjeddi is greatly appreciated for his interesting discussions and help with this work.

6. Author information

Email

Corresponding Author. *Hesam Taheri: hesam.taheri@univ-ubs.fr

Mohammad Mastali: muhammad.mastali@gmail.com

Mahroo Falah: mahroo.falah@betolar.com

Zahra Abdollahnejad: tolumahvash@gmail.com

Bahman Ghiassi: b.ghiassi@bham.ac.uk

Arnaud Perrot: arnaud.perrot@univ-ubs.fr

Shiho Kawashima: s-kawashima@columbia.edu

ORCID

*Hesam Taheri: 0000-0002-5508-5609

Mohammad Mastali: 0000-0001-8638-863X

Mahroo Falah: 0000-0001-9052-3320

Zahra Abdollahnejad: 0000-0002-5174-5833

Bahman Ghiassi: 0000-0003-4212-8961

Arnaud Perrot: 0000-0002-7105-4212

Shiho Kawashima: 0000-0002-3332-3936

7. References

1. Pierrehumbert R. There is no Plan B for dealing with the climate crisis. Bulltin of the atomic scientists 2019;75(5):215–221. https://doi.org/10.1080/00963402.2019.1654255.

2. Wu CJ, Zhang CJ, Yu DM, Li RG. Dissolving pulp from bamboo-willow. Cellulose 2018;25:777–785. https://doi.org/10.1007/s10570-017-1596-z.

3. Siró I, and Plackett D. Microfibrillated cellulose and new nanocomposite materials: a review. Cellulose 2010;17:459–494. https://doi.org/10.1007/s10570-010-9405-y.

4. Foster EJ, Moon RJ, Agarwal UP, Bortner MJ, Bras J, Camarero-Espinosa S et al. Current characterization methods for cellulose nanomaterials. ChemSocRev 2018:47:2609–2679. https://doi.org/10.1039/C6CS00895J.

5. Simão CD, Reparaz JS, Wagner MR, Graczykowski B, Kreuzer M et al. Optical and mechanical properties of nanofibrillated cellulose: Toward a robust platform for next-generation green technologies. Carbohydr Polym 2015;126:40–46. https://doi.org/10.1016/j.carbpol.2015.03.032.

6. Hietala M, Samuelsson E, Niinimäki J, Oksman K. The effect of pre-softened wood chips on wood fibre aspect ratio and mechanical properties of wood-polymer composites. Composites Part A 2011;42:2110–2116. https://doi.org/10.1016/j.compositesa.2011.09.021.

7. Taheri H and Samyn P. Rheological properties and processing of polymer blends with micro- and nanofibrillated cellulose. In: Hakeem KR, Jawaid M, Alothman OY (eds) Agricultural biomass based potential materials. Springer, Switzerland, 2015. p.259–291. https://doi.org/10.1007/978-3-319-13847-3_13.

8. Iwamoto S, Nakagaito AN, Yano H. Nano-fibrillation of pulp fibers for the processing of transparent nanocomposites. Appl. Phys. A 2007;89:461–466. https://doi.org/10.1007/s00339-007-4175-6.

9. Laitinen O, and Niinimäki J. Fractional study of the microfibrillated cellulose. Tappi J. 2014;13:49–55. https://doi.org/10.32964/TJ13.7.49.

10. Nechyporchuk O, Pignon F, Belgacem MN. Morphological properties of nanofibrillated cellulose produced using wet grinding as an ultimate fibrillation process. J. Mater. Sci 2015;50:531–541. https://doi.org/10.1007/s10853-014-8609-1.

11. Ho TTT, Zimmermann T, Caseri W. Preparation and characterization of cationic nanofibrillated cellulose from etherification and high shear disintegration processes. Cellulose 2011;18:1391–1406. https://doi.org/10.1007/s10570-011-9591-2.

12. Taheri H, and Samyn P. Effect of homogenization (microfluidization) process parameters in mechanical production of micro- and nanofibrillated cellulose on its rheological and morphological properties. Cellulose 2016;23:1221–1238. https://doi.org/10.1007/s10570-016-0866-5.

13. Johnson RK, Zink-Sharp A, Renneckar SH, Glasser GW. A new bio-based nanocomposite: Fibrillated TEMPO-oxidized celluloses in hydroxypropyl-cellulose matrix. Cellulose 2009;16:227–238. https://doi.org/10.1007/s10570-008-9269-6.

14. Lee H-J, Lee H-S, Seo J, Kang Y-H, Kim W, Kang TH-K. State-of-the-Art of Cellulose Nanocrystals and Optimal Method for their Dispersion for Construction-Related Applications. Applied Sciences. 2019;9(3):426(1-14). https://doi.org/10.3390/app9030426.

15. Ho TTT, Abe K, Zimmermann T, Yano H. Nanofibrillation of pulp fibers by twin-screw extrusion. Cellulose 2015;22:421–433. https://doi.org/10.1007/s10570-014-0518-6.

16. Hietala M, Rollo P, Kekäläinen K, Oksman K. Extrusion processing of green biocomposites: compounding, fibrillation efficiency and fiber dispersion. J Appl Polym Sci 2014;131(39981):1–9. https://doi.org/10.1002/app.39981.

17. Rol F, Karakashov B, Nechyporchuk O, Terrien M et al. Pilot-Scale Twin Screw Extrusion and Chemical Pretreatment as an Energy-Efficient Method for the Production of Nanofibrillated Cellulose at High Solid Content. ACS Sustainable Chem Eng 2017;5:6524−6531. https://doi.org/10.1021/acssuschemeng.7b00630.

18. Taheri H, Hietala M, Suopajärvi T, Liimatainen H, and Oksman K. One-Step Twin-Screw Extrusion Process to Fibrillate Deep Eutectic Solvent-Treated Wood to Be Used in Wood Fiber-Polypropylene Composites. ACS Sustainable Chem. Eng. 2021;9(2):883–893. https://dx.doi.org/10.1021/acssuschemeng.0c07750.

19. Taheri H, Hietala M, Oksman k. One-step twin-screw extrusion process of cellulose fibers and hydroxyethyl cellulose to produce fibrillated cellulose biocomposite. Cellulose 2020;27:8105–8119. https://doi.org/10.1007/s10570-020-03287-3.

20. Moon RJ, Martini A, Nairn J, Simonsen J, Youngblood J. Cellulose nanomaterials review: Structure, properties and nanocomposites. Chem. Soc. Rev. 2011;40:3941–3994. https://doi.org/10.1039/C0CS00108B.

21. Mejdoub R, Hammi H, Suñol J.J, Khitouni M, M'nif A, Boufi S. Nanofibrillated cellulose as nanoreinforcement in Portland cement: Thermal, mechanical and microstructural properties. J. Compos. Mater. 2017;51:2491–2503. https://doi.org/10.1177/0021998316672090.

22. Ardanuy Raso M, Claramunt Blanes J, Arévalo Peces R, Parés Sabatés F, Aracri E, Vidal Lluciá T. Nanofibrillated cellulose (NFC) as a potential reinforcement for high performance cement mortar composites. BioResources 2012;7:3883–3894.

23. Onuaguluchi O, Panesar D.K, Sain M. Properties of nanofibre reinforced cement composites. Constr. Build. Mater. 2014;63:119–124. https://doi.org/10.1016/j.conbuildmat.2014.04.072.

24. Tang Z, Huang R, Mei C, Sun X, Zhou D, Zhang X, Wu Q. Influence of Cellulose Nanoparticles on Rheological Behavior of Oil Well Cement-Water Slurries. Materials 2019;12(291):1–14. https://doi.org/10.3390/ma12020291.

25. Sun X, Wu Q, Zhang J, Qing Y, Wu Y, Lee S. Rheology, curing temperature and mechanical performance of oil well cement: Combined effect of cellulose nanofibers and graphene nano-platelets. Mater. Des. 2017;114:92–101. https://doi.org/10.1016/j.matdes.2016.10.050.

26. Sun X, Wu Q, Lee S et al. Cellulose nanofibers as a modifier for rheology, curing and mechanical performance of oil well cement. Sci Rep 2016;6(31654):1–9. https://doi.org/10.1038/srep31654.

27. Liu Z, Shao N, Wang Dm et al. Fabrication and properties of foam geopolymer using circulating fluidized bed combustion fly ash. Int J Miner Metall Mater 2014;21:89–94. https://doi.org/10.1007/s12613-014-0870-4.

28. Ramamurthy K, Kunhanandan Nambiar EK, Indu Siva Ranjani G. A classification of studies on properties of foam concrete. Cem. Concr. Compos. 2009;31:388–396. https://doi.org/10.1016/j.cemconcomp.2009.04.006.

29. Zhang Z, Provis JL, Reid A, Wang H. Mechanical, thermal insulation, thermal resistance and acoustic absorption properties of geopolymer foam concrete. Cem. Concr. Compos. 2015;62:97–105. https://doi.org/10.1016/j.cemconcomp.2015.03.013.

30. Lassinantti Gualtieri M, Cavallini A, Romagnoli M. Interactive powder mixture concept for the preparation of geopolymers with fine porosity. J. Euro. Ceram. Soc. 2016;36:2641–2646. https://doi.org/10.1016/j.jeurceramsoc.2016.03.030.

31. Strozi Cilla M, Colombo P, Raymundo Morelli M. Geopolymer foams by gelcasting. Ceram. Int. 2014;40:5723–5730. https://doi.org/10.1016/j.ceramint.2013.11.011.

32. Abdollahnejad Z, Pacheco-Torgal F, Félix T, Tahri W, Aguiar Barroso J. Mix design, properties and cost analysis of fly ash-based geopolymer foam. Constr. Build. Mater. 2015;80:18–30. https://doi.org/10.1016/j.conbuildmat.2015.01.063.

33. Hajimohammadi A, Ngo T, Mendis P, Kashani A, van Deventer JSJ. Alkali activated slag foams: the effect of the alkali reaction on foam characteristics. J. Cleaner Prod. 2017;147:330–339. https://doi.org/10.1016/j.jclepro.2017.01.134.

34. Mastali M, Kinnunen P, Karhu M, Abdollahnejad Z et al. Impacts of Casting Scales and Harsh Conditions on the Thermal, Acoustic, and Mechanical Properties of Indoor Acoustic Panels Made with Fiber-Reinforced Alkali-Activated Slag Foam Concretes. Materials 2019;12(825):1–26. https://doi.org/10.3390/ma12050825.

35. Cox WP, Merz EH. Correlation of dynamic and steady flow viscosities. J Polym Sci 1958;28(118):619–622. https://doi.org/10.1002/pol.1958.1202811812.

36. ASTM C78/C78M-16, Standard Test Method for Flexural Strength of Concrete (Using Simple Beam with Third-Point Loading), ASTM International, West Conshohocken, PA, 2016.

37. ASTM C109/C109M-20b, Standard Test Method for Compressive Strength of Hydraulic Cement Mortars (Using 2-in. or [50 mm] Cube Specimens), ASTM International, West Conshohocken, PA, 2020.

38. ASTM C567/C567M-14, Standard Test Method for Determining Density of Structural Lightweight Concrete, ASTM International, West Conshohocken, PA, 2014.

39. Roussel N. Rheological requirements for printable concretes. Cement and Concrete Research 2018;112:76–85. https://doi.org/10.1016/j.cemconres.2018.04.005.

40. Uchenna Okoronkwo M, Falzone G et al. Rheology-based protocol to establish admixture compatibility in dense cementitious suspensions. J. Mater. Civ. Eng. 2018;30(7)04018122:1–8. https://doi.org/10.1061/(ASCE)MT.1943-5533.0002277.

41. Sant G, Ferraris CF, Weiss J. Rheological properties of cement pastes: A discussion of structure formation and mechanical property development. Cement and Concrete Research 2008;38:1286–1296. https://doi.org/10.1016/j.cemconres.2008.06.008.

42. Nguyen TT, Bui HH, Ngo TD, Nguyen GD. Experimental and numerical investigation of influence of air-voids on the compressive behaviour of foamed concrete. Materials & Design 2017;130:103–119. https://doi.org/10.1016/j.matdes.2017.05.054.

43. Zhang X, Yang Q, Shi Y, Zheng G, Li Q, Chen H, Cheng X. Effects of different control methods on the mechanical and thermal properties of ultra-light foamed concrete. Construction and Building Materials 2020;262(120082):1–11. https://doi.org/10.1016/j.conbuildmat.2020.120082.

44. Raj A, Sathyan D, Mini KM. Physical and functional characteristics of foam concrete: A review. Construction and Building Materials 2019;221:787–799. https://doi.org/10.1016/j.conbuildmat.2019.06.052.

45. Zhihua P, Hiromi F, Tionghuan W. Preparation of high performance foamed concrete from cement, sand and mineral admixtures. J. Wuhan Univ. Technol. 2007;22:295–298. https://doi.org/10.1007/s11595-005-2295-4.

46. Falliano D, De Domenico D, Ricciardi G, Gugliandolo E. 3D-printable lightweight foamed concrete and comparison with classical foamed concrete in terms of fresh state properties and

mechanical strength. Construction and Building Materials 2020;254(119271):1–14. https://doi.org/10.1016/j.conbuildmat.2020.119271.

47. Oh J-A, Aakyiir M, Liu Y et al. Durable cement/cellulose nanofiber composites prepared by a facile approach. Cement and Concrete Composites 2022;125(104321):1–13. https://doi.org/10.1016/j.cemconcomp.2021.104321.